NASA Technical Memorandum 106877
ICOMP–95–6
AIAA–95–0680

Direct Computation of Sound Radiation by Jet Flow Using Large-Scale Equations

R. R. Mankbadi
Lewis Research Center
Cleveland, Ohio

S.H. Shih and D.R. Hixon
Institute for Computational Mechanics in Propulsion
Lewis Research Center
Cleveland, Ohio

L.A. Povinelli
Lewis Research Center
Cleveland, Ohio

Prepared for the
33rd Aerospace Sciences Meeting
sponsored by the American Institute of Aeronautics and Astronautics
Reno, Nevada, January 9–12, 1995

National Aeronautics and
Space Administration

Direct Computation of Sound Radiation by Jet Flow Using Large-Scale Equations

R. R. Mankbadi*
NASA Lewis Research Center
Cleveland, Ohio 44135

S. H. Shih** and D. R. Hixon**
Institute for Computational Mechanics in Propulsion
NASA Lewis Research Center
Cleveland, Ohio 44135

L. A. Povinelli***
NASA Lewis Research Center
Cleveland, Ohio 44135

Abstract

Jet noise is directly predicted using large-scale equations. The computational domain is extended in order to directly capture the radiated field. As in conventional large-eddy-simulations, the effect of the unresolved scales on the resolved ones is accounted for. Special attention is given to boundary treatment to avoid spurious modes that can render the computed fluctuations totally unacceptable. Results are presented for a supersonic jet at Mach number 2.1.

1. Introduction

The recent growing interest in turbulence noise is largely due to efforts to develop a high-speed civil transport plane. The success of this new technology is contingent upon reducing its jet exhaust noise.The jet noise is generated by the time dependent flow fluctuations in the near field which are associated with pressure fluctuations that propagate to the far field producing the radiated sound. In theory, direct numerical simulation (DNS) based on the compressible Navier-Stokes equations provide both the flow fluctuations and the acoustic field. However, the resolution requirement for high-Reynolds number turbulent flows makes direct numerical simulation impractical due to current computer limitations. In large-eddy simulations, the full navier-Stokes equations are solved, while realizing that the smaller scales of turbulence can not be resolved for high-Reynolds number turbulent flows. Modelling is used to account for the effect of these unresolved scales on the resolved ones. It is believed that the large scale structure is more efficient than the small scale structure in radiating sound [1-5]. This indicates that it is appropriate to perform large-eddy simulations to accurately capture the large scales of motion while modelling the sub-grid scale turbulence.

The use of large-eddy simulations (LES) as a tool for prediction of the jet noise source has been proposed by Mankbadi et al. [6]. The fluctuating sound source in the near field was then used to obtain the far field sound through the application of Lighthill's theory. It was shown [6] that because of the non-compactness of the source and the need to account for the retarded time, accurate application of Lighthill's theory requires, in turn, prohibitive computer storage. The present work is concerned with avoiding such techniques via direct extension of the computational domain to capture the radiated field. Large-scale equations are solved for both the sound and the acoustic fields. The Smagorinsky's model is used for simplicity. But further attention is needed for modelling the effect of the smaller scales on the larger ones, particularly for the acoustic disturbance. Careful attention is given in this paper to the boundary treatment, which is the main issue in predicting an accurate acoustic field.

2. Governing Equations

The flow field of a supersonic jet is governed by the compressible Navier-Stokes equations, and can be decomposed into filtered and residual fields, namely

* Senior scientist and technical leader, CAA, Associate fellow AIAA
** Senior research associate, Member AIAA
*** Acting Chief, Internal Fluid Mechanics Division, Fellow, AIAA

$$f = \bar{f} + f'' \tag{1}$$

where an overbar denotes the resolved (filtered) field and a (") denotes the unresolved (subgrid) one. The mean of the filtered field is the mean of the total field. Upon substituting this splitting in the full Navier-Stokes equations, the filtered compressible Navier-Stokes equations in cylindrical coordinates takes the form

$$\frac{\partial Q}{\partial t} + \frac{\partial F}{\partial x} + \frac{1}{r}\frac{\partial}{\partial r}(rG) = S \tag{2}$$

where

$$Q = \left[\bar{\rho},\ \bar{\rho}\tilde{u},\ \bar{\rho}\tilde{v},\ \bar{\rho}\tilde{E}\right]^T \tag{3}$$

$$F = \begin{bmatrix} \bar{\rho}\tilde{u} \\ \bar{p} + \bar{\rho}\tilde{u}^2 - \bar{\sigma}_{xx} - \tau_{xx} \\ \bar{\rho}\tilde{u}\tilde{v} - \bar{\sigma}_{xr} - \tau_{xr} \\ \bar{\rho}\tilde{u}\tilde{I} - \tilde{u}\bar{\sigma}_{xx} - \tilde{v}\bar{\sigma}_{xr} - k\frac{\partial}{\partial x}\tilde{T} - c_v q \end{bmatrix} \tag{4}$$

$$G = \begin{bmatrix} \bar{\rho}\tilde{v} \\ \bar{\rho}\tilde{u}\tilde{v} - \bar{\sigma}_{xr} - \tau_{xr} \\ \bar{p} + \bar{\rho}\tilde{v}^2 - \bar{\sigma}_{rr} - \tau_{rr} \\ \bar{\rho}\tilde{v}\tilde{I} - \tilde{u}\bar{\sigma}_{xr} - \tilde{v}\bar{\sigma}_{rr} - k\frac{\partial}{\partial r}\tilde{T} - c_v q \end{bmatrix} \tag{5}$$

$$S = \frac{1}{r}\begin{bmatrix} 0 \\ 0 \\ \bar{p} - \bar{\sigma}_{\phi\phi} - \tau_{\phi\phi} \\ 0 \end{bmatrix} \tag{6}$$

Here Q is the unknown vector, F and G are the fluxes in the x and r directions, respectively; S is the source term that arises in cylindrical polar coordinates; and k is thermal conductivity. The total enthalpy is I, the total energy is E, and σ_{ij} are the viscous stresses. This system of equations is coupled with the equation of state for a perfect gas. Here, a tilde denotes Favre filtering,

$$\tilde{f} = \frac{\overline{\rho f}}{\bar{\rho}} \tag{7}$$

The unresolved stresses τ_{ij} appearing in equations (4-6) need to be modeled.

3. Subgrid-Scale Modelling

The Smagorinsky's model [7] was chosen to represent the effect of the subgrid-scale turbulence stresses.

$$\tau_{ij} = k_g(\delta_{ij}/3) - 2\rho\nu_R\left(\tilde{S}_{ij} - \frac{1}{3}\delta_{ij}\tilde{S}_{mm}\right) \tag{8}$$

where k_g is the kinetic energy of the residual turbulence. The strain rate of the resolved scale is given by

$$\tilde{S}_{ij} = \frac{1}{2}\left(\frac{\partial\tilde{u}_i}{\partial x_j} + \frac{\partial\tilde{u}_j}{\partial x_i}\right) \tag{9}$$

The summation S_{mm} is zero for incompressible flow, ν_R is the effective viscosity of the residual field,

$$\nu_R = (C_s\Delta_f)^2 \cdot \sqrt{2S_{mn}S_{mn}} \tag{10}$$

and Δ_f is the filter width given by

$$\Delta_f = (\Delta_x\Delta_r)^{1/2} \tag{11}$$

For the heat equation, Edison [8] proposed the eddy viscosity model

$$q = \bar{\rho}\frac{\nu_R}{Pr_t}\frac{\partial\tilde{T}}{\partial x_k} \tag{12}$$

where Pr_t is the subgrid-scale turbulent Prandtl number, which can be taken as 0.5. Smagorinsky's constant C_s in equation (10) is given by Reynolds [9] as 0.23. In the presence of mean shear, however, this value was found to cause excessive damping of large-scale fluctuations, and in his simulation of turbulent channel flow, Deardorff [10] used $C_s = 0.1$. Piomelli et al. [11] found the optimum value of C_s to be 0.1. This value was used herein.

Although Smagorinsky's model is one of the simplest models, it assumes a balance between the subgrid-scale energy production and its dissipation. This balance may not be true in several situations. Further work is needed for developing more appropriate subgrid-scale models for jet noise predictions.

4. Numerical Scheme

The importance of the dispersion and dissipation of a given scheme, used in connection with the computational aeroacoustics, was highlighted by Hardin [12]. Both effects are crucial in computational aeroacoustics, and can render the computed unsteady part of the solution completely unacceptable. As such, high-order accurate schemes are required for problems in computational aeroacoustics.

A fourth-order accurate in space, second-order accurate in time scheme is used, which is an extension of the MacCormack scheme by Gottlieb and Turkel [13]. Man-

kbadi et al. [6] used this scheme to study the structure of axisymmetric supersonic jet flow. Ragab and Sheen [14], and Farouk, Oran and Kailasanath [15] have also successfully applied this scheme for the study of nonlinear instability problems in plane shear layers. Sankar, Reddy and Hariharan [16] performed a comparative study of various numerical schemes for aeroacoustics applications, and found that this scheme offers high spatial accuracy. In this scheme, the operator is split into two one-dimensional operators and applied in a symmetric way to avoid biasing of the solution:

$$Q^{n+2} = L_{2x}L_{2r}L_{1r}L_{1x}Q^{n} \tag{13}$$

where L represents the one-dimensional operator. Each operator consists of a predictor and a corrector steps, and each step uses one-sided differencing:
Predictor:

$$Q_i^{n+\frac{1}{2}} = Q_i^n - \frac{\Delta t}{6\Delta x}\left(7F_i - 8F_{i-1} + F_{i-2}\right)^n \tag{14}$$

Corrector:

$$Q_i^{n+1} = \frac{1}{2}\left[Q_i^n + Q_i^{n+\frac{1}{2}} + \frac{\Delta t}{6\Delta x}\left(7F_i - 8F_{i+1} + F_{i+2}\right)^{n+\frac{1}{2}}\right] \tag{15}$$

and likewise for the radial direction. The scheme becomes fourth-order accurate in the spatial derivatives when alternated with symmetrical variants. Let L_1 be the one-dimensional operator with forward difference in the predictor and backward difference in the corrector, then L_2 will be the one-dimensional operator with backward difference in the predictor and forward difference in the corrector. At the computational boundaries, flux quantities outside the boundaries are needed to compute the spatial derivatives, and these can be obtained using third-order extrapolation based on data from the interior of the domain.

5. Boundary Conditions

Special attention is given herein to boundary treatment in order to avoid non-physical oscillations that can render the computed acoustic field unacceptable. Several boundary treatments were considered [17,18]. The boundary treatment discussed below were found to be stable, non-reflecting, and most suitable for the present jet computations.

5.1 Inflow Boundary

At the inflow boundary (x=0), the radial boundary is split into hydrodynamic disturbance and radiation regimes, which are treated differently according to the physics involved.

5.1.1 Hydrodynamic Disturbance Regime

At the inflow boundary, a small disturbance is introduced. This disturbance is assumed to be mainly hydrodynamic in nature, and is specified from the centerline to r/D=2. To a first approximation, the inflow disturbances is assumed to be small such that the linear stability theory applies. A normal mode decomposition for the disturbance is assumed in the form:

$$\left[u'\ v'\ p'\ \rho'\right] = \Re\left\{\Phi(r)\, e^{i(\alpha x - \omega t)}\right\} \tag{16}$$

The governing equations in this case can be reduced to Orr-Sommerfeld equation, which are solved to obtain the complex wave number α as the eigenvalue corresponding to the frequency ω and the radial functions $\Phi(r)$ as the corresponding eigenfunctions.

$$\Phi(r) = \left[\hat{u}(r)\ \hat{v}(r)\ \hat{p}(r)\ \hat{\rho}(r)\right] \tag{17}$$

To obtain the disturbance solution a mean flow must be specified. In the present work, the analytical functions proposed by Tam and Burton [19] to fit the experimental data of Troutt and McLaughlin [20] were used. The mean axial velocity is given by

$$U = 1 \qquad \text{for } r<h$$

$$U = \exp\left[-\ln(2)\left(\frac{r-h(x)}{b(x)}\right)^2\right] \quad \text{for } r>h \tag{18}$$

where b(x) is the half-width of the annular mixing layer, and is fitted to the experimental data. The radius of the potential core, h(x), is related to b(x) through the conservation of momentum:

$$\int_0^\infty \rho U^2 r dr = \frac{1}{2} \tag{19}$$

Velocities are normalized by the streamwise velocity at the jet exit centerline; density by the exit centerline density; and distances by the nozzle radius. The static pressure is uniform in the radial direction. The total temperature is assumed uniform, which provides the distribution for the static temperature

$$T_0 = T + \frac{U^2}{2\rho c_p} \tag{20}$$

where c_p is the specific heat under constant pressure. The

density is obtained from the equation of state.

For the supersonic regime, all characteristics travel in the flow direction. Thus the primitive variables are given at x=0 as outlined above. An extrapolation is needed for the two points outside the domain (x<0). Rather than using the conventional polynomial extrapolation, we choose the extrapolation function to fit the linear growth rate, namely:

$$u(x,r) = Ae^{\beta x}\Re\{\hat{u}(r)e^{i(\alpha x-\omega t)}\} \qquad (21)$$

where β represents the growth rate that can be obtained either from the linear theory or from the interior solution.

In the subsonic regime, the following three characteristics are specified according to the linear stability solution:

$$\begin{aligned} p_t + \rho c u_t &= C_1 \\ p_t - c^2\rho &= C_2 \\ \rho c v_t &= C_3 \end{aligned} \qquad (22)$$

The fourth characteristic is outgoing and is obtained from the interior solution:

$$p_t - \rho c u_t = C_4 \qquad (23)$$

The four characteristic equations are then solved together to obtain the time derivatives of the variables, which are used to update the solution at the inflow boundary.

5.1.2 Radiation regime

In the radiation regime (r/D>2), the conventional acoustic radiation condition applies:

$$Q_t = -\Gamma(\theta)\left[\frac{x}{R}Q_x + \frac{r}{R}Q_r + \frac{Q}{R}\right] \qquad (24)$$

where:

$$\begin{aligned} Q &= [u\ v\ p\ \rho] \\ R &= \sqrt{x^2+r^2} \\ \Gamma(\theta) &= c\left[\frac{x}{R}M + \sqrt{1-\left(\frac{r}{R}M\right)^2}\right] \end{aligned} \qquad (25)$$

and M is the local Mach number, c is the sonic velocity. The spatial derivatives which appear in equation (24) are evaluated in an identical manner as the inner flow derivatives.

5.2 Outflow Boundary

The outflow treatment is based on the asymptotic analysis of the linearized equations as given by Tam and Webb [21]. The pressure condition is the same as that obtained by Bayliss and Turkel [22], Enquist and Majda [23], and Hariharan and Hagstrom [24], namely:

$$p_t = -\Gamma(\theta)\left[\frac{x}{R}p_x + \frac{r}{R}p_r + \frac{p}{R}\right] \qquad (26)$$

However, for updating the rest of the primitive variables, Tam and Webb have shown that the momentum and continuity equations should be used to account for the presence of entropy and vorticity waves at the outflow boundary. The spatial differencing used in the inner code is employed to evaluate the derivatives which appear in equation (26).

For the outflow regime of large radius with the local Mach number less than 0.01, the outflow condition is replaced by the conventional radiation condition of Section 5.1.2.

5.3 Outer Radial Boundary

At the outer radial boundary ($r=r_{max}$, $0<x<x_{max}$), the conventional radiation boundary condition of Section 5.1.2. is used.

5.4 Centerline Boundary

The results presented herein are for axisymmetric disturbance, for which the boundary condition at r=0 can be stated as

$$\begin{aligned} \frac{\partial}{\partial r}[u\ p\ \rho] &= 0 \\ v &= 0 \end{aligned} \qquad (27)$$

The centerline treatment for non-axisymmetric disturbances is not obvious, and is addressed in a separate paper by Shih et al [25]

6. Results and Discussion

The numerical results of the flow and acoustic fields of a cold, nearly perfectly expanded axisymmetric supersonic jet of Mach number 2.1 will be presented. The total temperature of the jet is 294° K, and the jet exit pressure is 0.0515 atm. The Reynolds number based on exit conditions is approximately 70000. In the present calculation, the jet is excited at a Strouhal number of 0.2 with the Strouhal number defined as $St=fD/U_o$, where D is the nozzle exit diameter and U_o is the jet exit centerline velocity. The computed results will be compared with the analytical solutions of Tam and Burton [19] and the experimental measurements of Troutt and McLaughlin [20].

The computational domain for this problem extends axially from x/D=2.5 to x/D=35, and radially from centerline to r/D=32, as shown in figure 1. Due to the steep mean flow gradient encountered at the jet exit, the computational grid was begun at an axial distance x/D=2.5 from the actual jet exit. The appropriate boundary treatments are also indicated on this figure. The computational grid consists of 391 equally spaced points in the axial direction. In the radial direction, 150 points are used and stretched between centerline and r/D=2.5 with concentration of grid points around r/D=0.5. Between r/D=2.5 and r/D=16, 130 equally spaced points are used with a spacing equal to that of the last stretched points.

Figure 2 shows the instantaneous distribution of ρ, p, u and v. As one can see that the solution is clean from boundary reflections. The wave-like nature of the flow field is evident The sound pattern seems to peak at angle influenced by the streamwise position where the fluctuation reaches a maximum. The spreading of the jet can be seen in the instantaneous axial velocity and density distributions.

Figure 3 shows the mean flow Mach number profiles at various streamwise positions. The computed Mach number profiles indicate the spreading of the jet, but it is underpredicted when compared with the measurements. This might be attributed to the fact that the present calculation is axisymmetric, and the uncertainty of the subgrid-scale model used as was discussed in section 3. Secondly, the present inflow boundary treatment might need to be modified to allow for specifying entrainment.

Figure 4 shows contours of the root-mean-square values of the axial momentum and pressure distributions. The preferred emission is evident in the figure.

Figures 5 and 6 show the axial development of the axial momentum and pressure fluctuations on the nozzle lip line. The computed results are compared with the measurements of Troutt and McLaughlin [20]. As can be seen in this figure, the computed curve peaks at about 5 diameters downstream of the measured peak. It implies that the noise source of the calculated results is located somewhat downstream of the measured peak. In the experiment of Troutt and McLaughlin [20], instability waves were excited by a single point glow discharge mounted flush near the nozzle exit. However, as pointed out by Troutt and McLaughlin, the measurements showed that the excited motion of the jet is dominated by the first helical mode in addition to the axisymmetric mode. It is expected that the peak of the curve would move upstream if the axisymmetric and the helical modes excitations are applied simultaneously.

Figures 7 and 8 shows radial profiles of the axial momentum and pressure fluctuations in the jet for several downstream positions. The radial peak of the fluctuation amplitude moves toward the jet centerline, and the width of the shear layer increases with downstream locations. The profiles at x/D=5 in both figures are typical of the eigenfunctions of linear stability analysis.

Figures 9 and 10 show the frequency spectra of axial velocity and pressure at several downstream locations in the center of shear layer. The spectra indicates that the dominant frequency is that of the fundamental forcing frequency and the subsequent harmonics. The amplitudes of the fundamental and harmonics decay at downstream location, but not so rapidly as observed in the measurements.

Figure 11 shows the sound pressure level distribution in the far field for the present calculation, the axisymmetric mode of Tam and Burton [19], and the experimental measurements of Troutt and McLaughlin [20]. It is seen that the patterns of the sound pressure level contours are all qualitatively similar. The lobed appearance of figure 11a indicates that the present calculation predicts a strong noise radiation in a direction at approximately 30° from the location of the maximum fluctuation. However, the present results show a downstream shift of the lobes when compared to the analytical solutions and experimental measurements. As pointed out in the discussion of figure 5, the calculated disturbance peaks downstream of the measured data and the spreading is underpredicted. This implies that the field shape of the calculated sound pressure level would be displaced downstream relative to Troutt and McLaughlin's observations.

Figure 12 shows the calculated and measured sound field directivity at a circle of radius 24D with center at the jet exit centerline. The angle is measured from the jet exit centerline. The calculated peak occurs around 15 degrees, which is smaller than the measured one. This is due to the downstream shifting of the field pattern of the overall sound pressure level, as was discussed in figure 11.

7. Conclusions

Direct prediction of jet noise seems to be feasible for the axisymmetric case. In the large-scale simulation presented herein, the computational domain is extended to capture the radiated field, while modelling the effect of the smaller scales on the larger ones. However, careful

attention is needed as was done herein, to boundary treatment, which becomes a serious issue in computing the acoustic field. The only limitation of large-scale simulation as compared to direct numerical simulation is that the smaller scale is not predicted. However, it is believed that the larger scales are more effective than the smaller scales in emitting sound. In conventional large-eddy simulation, the objective is the prediction of the mean flow field. But, herein, the objective is the fluctuation field. Thus, careful attention is given to the algorithm used and boundary treatment for handling wave-type solutions.

Results presented for the axisymmetric field of Mach number 2.1 jet with single frequency disturbance at the inflow exhibit features consistent with the observations. Three dimensional effects are needed to produce jet spreading rate consistent with the observation. The small scale modelling might also need crucial attention, not only for adequate spreading of the jet, but also for extension to acoustic disturbances. The predicted acoustic field, however, seems to be in qualitative agreement with the observation. As previously pointed out [19,20], the azimuthal modes seem to be responsible for a higher peak emission angle as compared to the axisymmetric case.

References

1. Seiner, J. M., McLaughlin, D. K. and Liu, C. H., "Supersonic Jet Noise Generated by Large-Scale Instabilities," NASA TP-2072, September, 1982.
2. Zaman, K. B. M. Q., "Flow Field and Near and Far Sound Field of a Subsonic Jet," Journal of Sound and Vibration, Vol. 106, pp. 1-6, 1986.
3. Mankbadi, R. R. and Liu, J. T. C., "Sound Generated Aerodynamically Revisited: Large-Scale Structures in a Turbulent Jet as a Source of Sound," Philos. Trans. Royal Society of London A, Vol. 311, pp. 183-217, 1984.
4. Mankbadi, R. R., "The Self Noise from Ordered Structures in a Low Mach Number Jet," Journal of Applied Mechanics, Vol. 57, pp. 241-246, 1990.
5. Mankbadi, R. R., "Dynamics and Control of Coherent Structure in Turbulent Jets," Applied Mechanics Reviews, Vol. 45, No. 6, pp. 219-247, 1992.
6. Mankbadi, R. R., Hayder, M. E. and Povinelli, L. A., "The Structure of Supersonic Jet Flow and Its Radiated Sound," AIAA Journal, Vol. 32, pp. 897-906, 1994.
7. Smagorinsky, J., "General Circulation Experiments with the Primitive Equations, I. The Basic Experiment," Monthly Weather Review, Vol. 91, pp. 99-164, 1963.
8. Edison, T. M., "Numerical Simulation of Turbulent Rayleigh-Bernard Problem Using Numerical Subgrid Modelling," Journal of Fluid Mechanics, Vol. 158, pp. 245-268, 1985.
9. Reynolds, W. C., "The Potential and Limitations of Direct and Large Eddy Simulations," Whither Turbulence?: Turbulence at the Crossroads, Proceedings of the Workshop, J. L. Lumley, ed., Springer-Verlag, New York, pp. 313-342, 1989.
10. Deardorff, J. W., "Numerical Study of Three-Dimensional Turbulent Channel Flow at Large Reynolds Number," Journal of Fluid Mechanics, Vol. 41, pp. 453-480, 1970.
11. Piomelli, U., Moin, P., and Ferziger, J. H., "Model Consistency in Large Eddy Simulation of Turbulent Channel Flows," Physics of Fluids, Vol. 31, pp. 1884-1891, 1988.
12. Hardin, J. C., "Recent Insights into Computational Aero-Acoustics," in Computational Aero- and Hydro-Acoustics, edited by R. R. Mankbadi, A. S. Lyrintzis, O. Baysal, L. A. Povinelli, M. Y. Hussaini, FED-Vol. 147, pp. 1, 1993.
13. Gottlieb, D. and Turkel, E., "Dissipative Two-Four Methods for Time-Dependent Problems," Mathematics of Computation, Vol. 30, No. 136, pp. 703-723, 1976.
14. Ragab, S. A. and Sheen, S., "The Nonlinear Development of Supersonic Instability Waves in a Mixing Layer," Physics of Fluids A, Vol. 4, pp. 553-566, 1991.
15. Farouk, B., Oran, E. S. and Kailasanath, K., "Numerical Simulations of the Structure of Supersonic Shear Layers," Physics of Fluids A, Vol. 3, pp. 2786-2798, 1991.
16. Sankar, L. N., Reddy, N. N. and Hariharan, N., "A Comparative Study of Numerical Scheme for Aero-Acoustic Applications," in Computational Aero- and Hydro-Acoustics, edited by R. R. Mankbadi, A. S. Lyrintzis, O. Baysal, L. A. Povinelli, M. Y. Hussaini, FED-Vol. 147, pp. 1, 1993.
17. Hixon, R., Shih, S. H., and Mankbadi, R. R., "Evaluation of Boundary Conditions for Computational Aeroacoustics." AIAA Paper 95-0160, Reno, Nevada, Jan. 1995.
18. Scott, J. N., Mankbadi, R. R., Hayder, M. E., and Hariharan, S. I., "Outflow Boundary Conditions for the Computational Analysis of Jet Noise," AIAA Paper 93-4366, 1993.
19. Tam, C. K. W. and Burton, D. E., "Sound Generated by Instability Waves of Supersonic Flows, Part 2: Axisymmetric Jets," Journal of Fluid Mechanics, Vol. 138, 1984, PP. 273-295, 1984.
20. Troutt, T. R. and McLaughlin, D. K., "Experiments on the Flow and Acoustic Properties of a Moderate

Reynolds Number Supersonic Jet," Journal of Fluid Mechanics, Vol. 116, PP 123-156, 1982.
21. Tam, C. K. W. and Webb, J. C., "Dispersion-Relation-Preserving Finite Difference Schemes for Computational Acoustics," Journal of Computational Physics, Vol. 107, pp. 262-281, 1993.
22. Bayliss, A. and Turkel, E., "Far Field Boundary Condition for Compressible Flows," Journal of Computational Physics, Vol. 48, pp. 182-199, 1982.
23. Enquist, B. and Majda, A., "Radiation Boundary Conditions for Acoustic and Elastic Wave Calculations," Communications on Pure and Applied Mathematics, Vol. 32, No. 3, pp. 313-357, 1979.
24. Hagstrom, t. and Hariharan, S. I., "Far Field Expansion for Anisotropic Wave Equations," Computational Acoustics, Vol. 2, 1990.
25. Shih, S. H., Hixon, R. and Mankbadi, R. R.,"Three Dimensional Structure in a Supersonic Jet: Behavior Near Centerline," AIAA Paper 95-0681, Reno, Nevada, January, 1995.

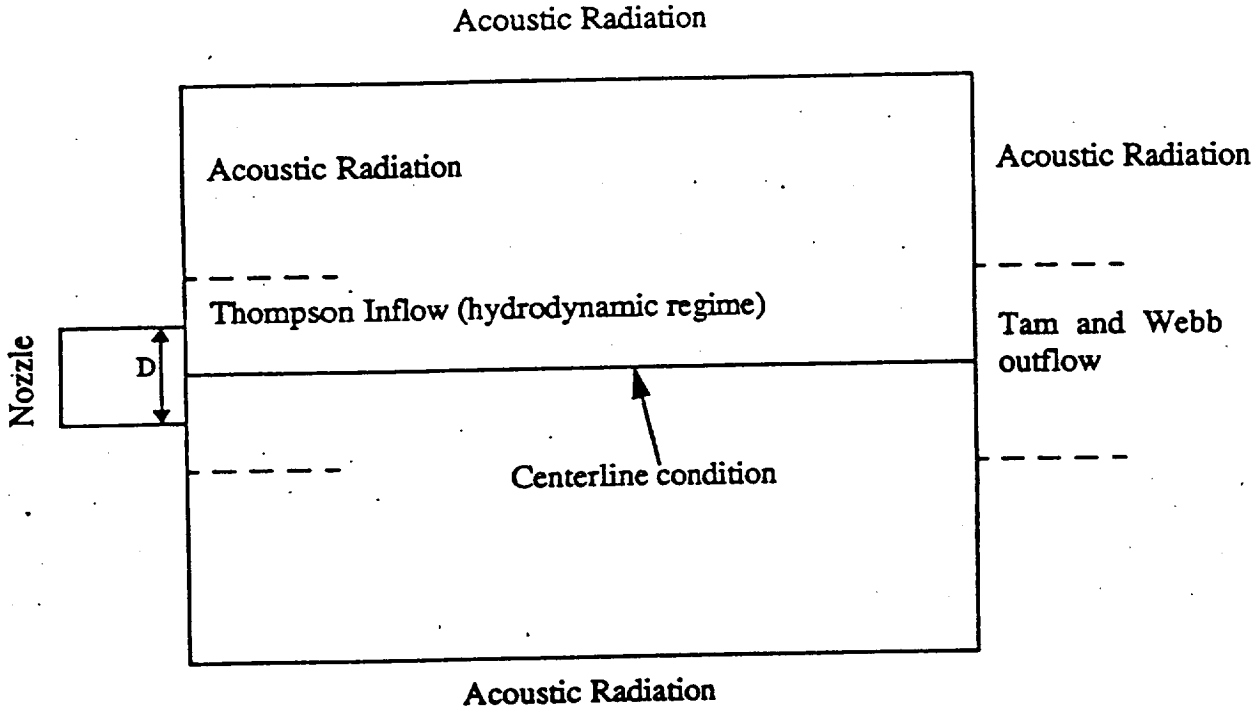

Fig. 1 Computational Domain

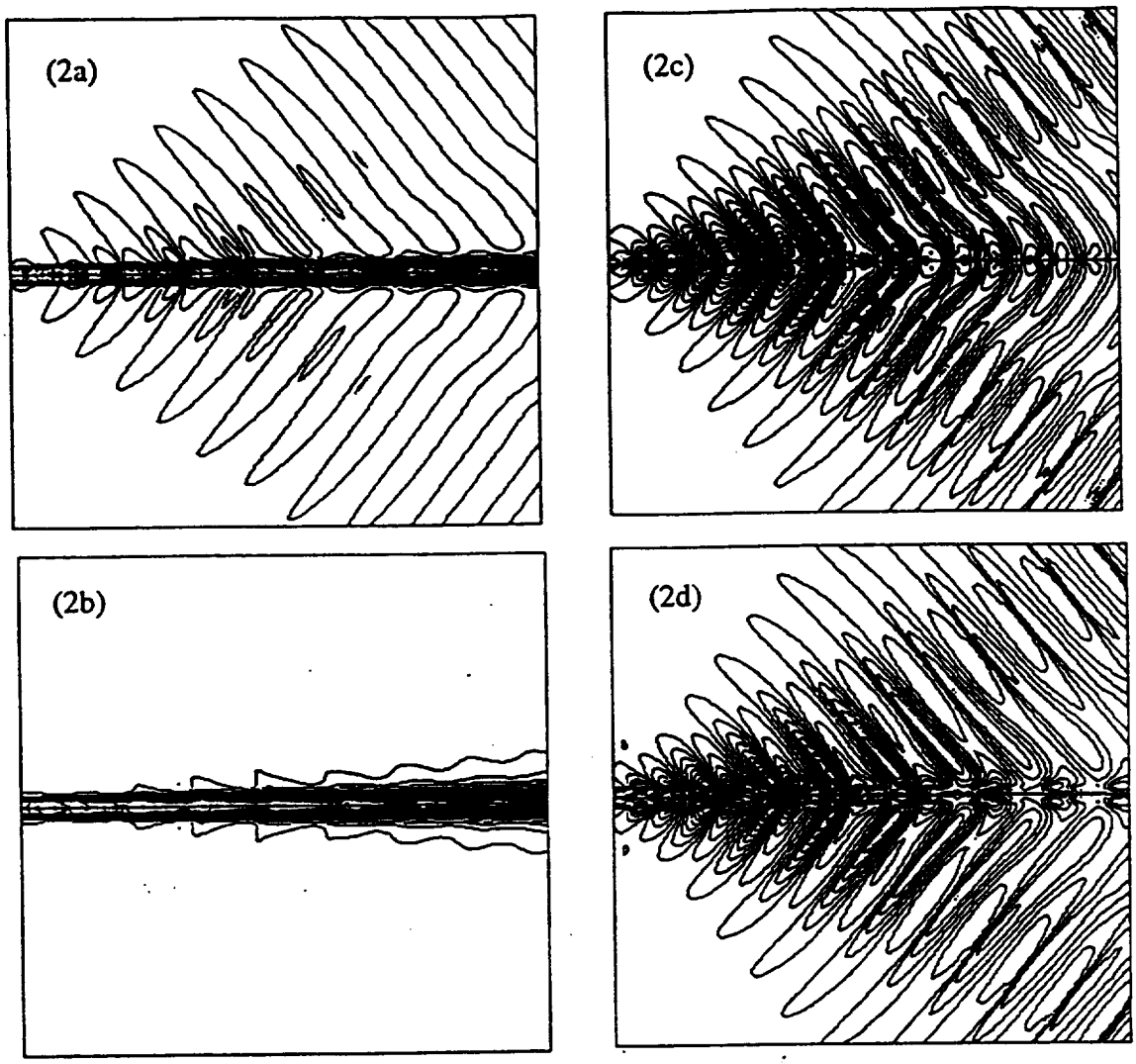

Fig. 2 Instantaneous distributions of (a) density (b) axial velocity (c) pressure (d) radial velocity.

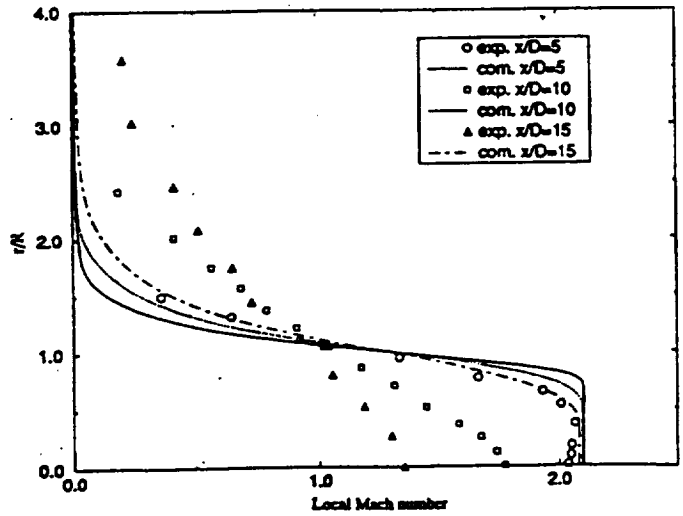

Fig. 3 Mean Mach number profiles at various streamwise positions.

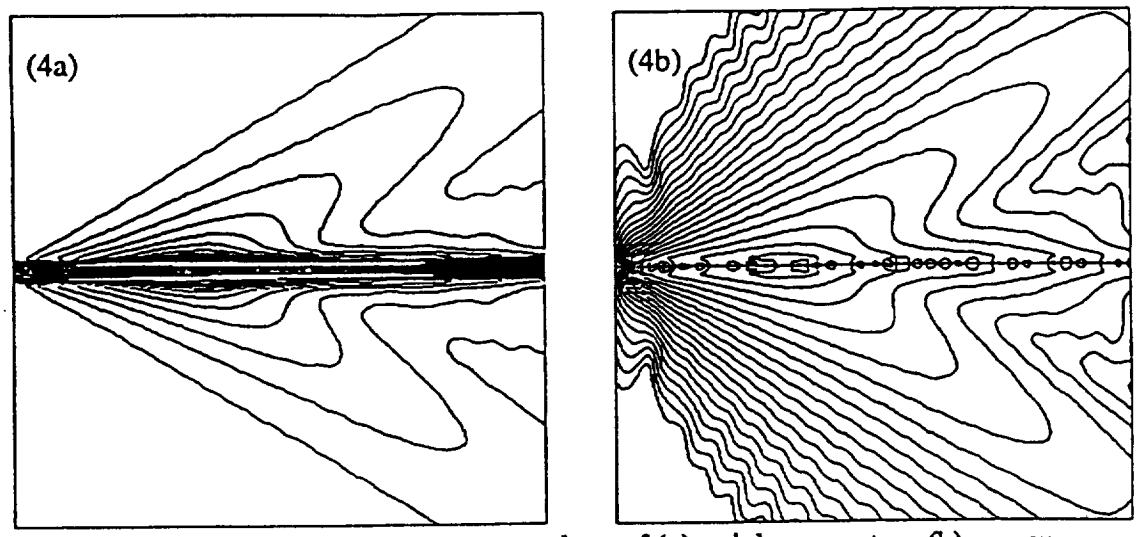

Fig. 4 Contours of root-mean-square values of (a) axial momentum (b) pressure.

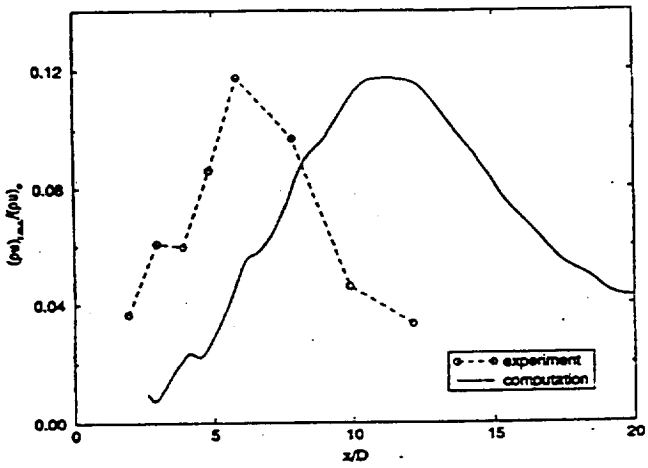

Fig. 5 Root mean square values of axial momentum at r/R=1.

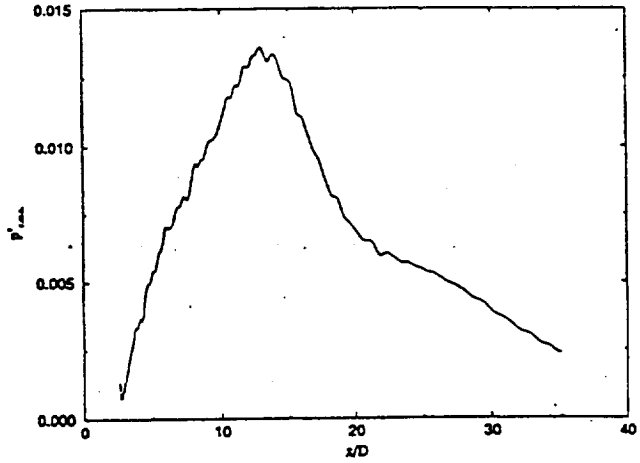

Fig. 6 Root mean square value of pressure at r/R=1.

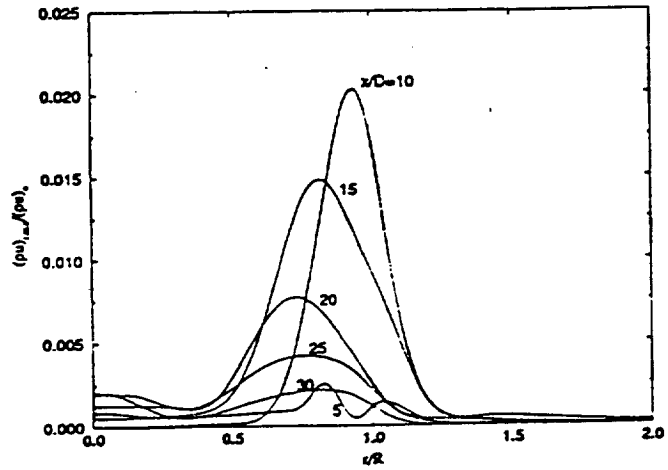

Fig. 7 Radial profiles of root-mean-square values of axial momentum.

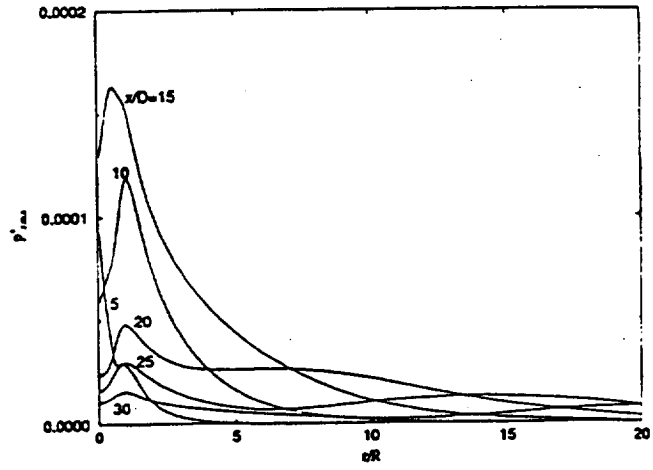

Fig. 8 Radial profiles of root-mean-square values of pressure.

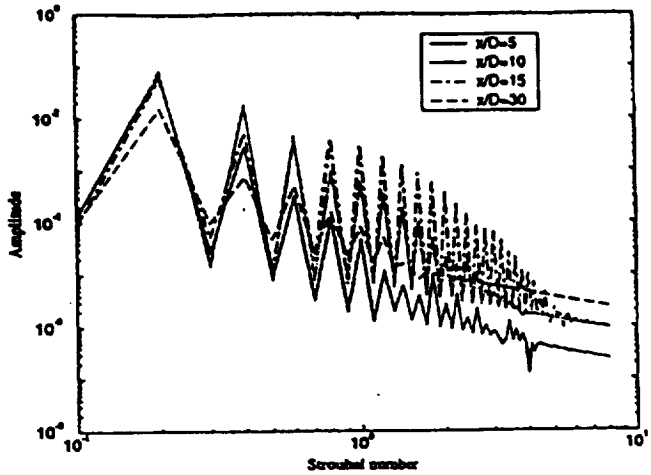

Fig. 9 Axial velocity spectra in the shear layer, r/D=0.5.

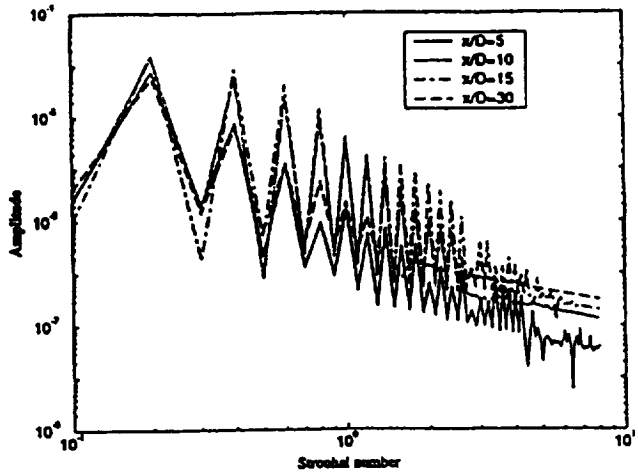

Fig. 10 Pressure spectra in the shear layer, r/D=0.5.

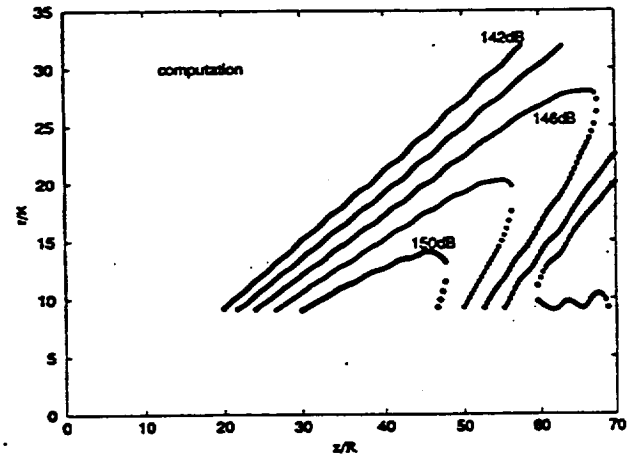

Fig. 11a Sound pressure level contours for present calculation.

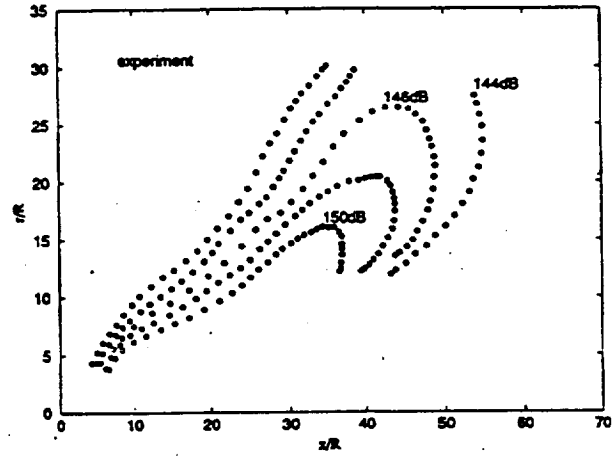

Fig. 11b Sound pressure level contours for Troutt and McLaughlin's experiment.

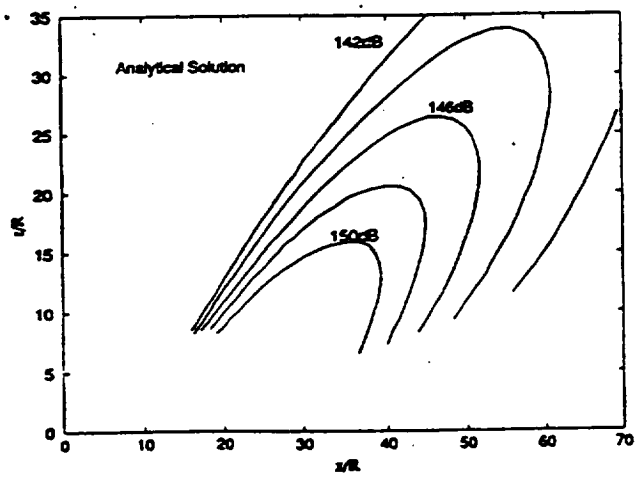

Fig. 11c Sound pressure level contours for Tam and Burton's analytical solution.

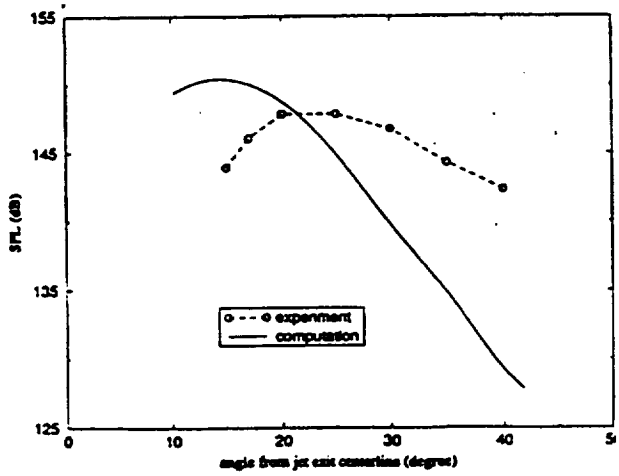

Fig.12 Directivity of jet noise at $\overline{R}/D=24$.

REPORT DOCUMENTATION PAGE

Form Approved
OMB No. 0704-0188

1. AGENCY USE ONLY (*Leave blank*)	2. REPORT DATE	3. REPORT TYPE AND DATES COVERED
	March 1995	Technical Memorandum

4. TITLE AND SUBTITLE
Direct Computation of Sound Radiation by Jet Flow Using Large-Scale Equations

5. FUNDING NUMBERS
WU-505-90-5K

6. AUTHOR(S)
R.R. Mankbadi, S.H. Shih, D.R. Hixon, and L.A. Povinelli

7. PERFORMING ORGANIZATION NAME(S) AND ADDRESS(ES)
National Aeronautics and Space Administration
Lewis Research Center
Cleveland, Ohio 44135-3191

8. PERFORMING ORGANIZATION REPORT NUMBER
E-9503

9. SPONSORING/MONITORING AGENCY NAME(S) AND ADDRESS(ES)
National Aeronautics and Space Administration
Washington, D.C. 20546-0001

10. SPONSORING/MONITORING AGENCY REPORT NUMBER
NASA TM-106877
ICOMP-95-6
AIAA-95-0680

11. SUPPLEMENTARY NOTES
Prepared for the 33rd Aerospace Sciences Meeting sponsored by the American Institute of Aeronautics and Astronautics, Reno, Nevada, January 9-12,1995. R.R. Mankbadi, NASA Lewis Research Center; S.H. Shih, and D.R. Hixon, Institute for Computational Mechanics in Propulsion, NASA Lewis Research Center (work funded under Cooperative Agreement NCC3-370). ICOMP Program Director, L.A. Povinelli, organization code 2600, (216) 433-5818.

12a. DISTRIBUTION/AVAILABILITY STATEMENT
Unclassified - Unlimited
Subject Category 34

This publication is available from the NASA Center for Aerospace Information, (301) 621-0390.

12b. DISTRIBUTION CODE

13. ABSTRACT (*Maximum 200 words*)

Jet noise is directly predicted using large-scale equations. The computational domain is extended in order to directly capture the radiated field. As in conventional large-eddy-simulations, the effect of the unresolved scales on the resolved ones is accounted for. Special attention is given to boundary treatment to avoid spurious modes that can render the computed fluctuations totally unacceptable. Results are presented for a supersonic jet at Mach number 2.1.

14. SUBJECT TERMS	15. NUMBER OF PAGES
Large-scale simulation; Jet noise; Boundary conditions	12
	16. PRICE CODE: A03

17. SECURITY CLASSIFICATION OF REPORT	18. SECURITY CLASSIFICATION OF THIS PAGE	19. SECURITY CLASSIFICATION OF ABSTRACT	20. LIMITATION OF ABSTRACT
Unclassified	Unclassified	Unclassified	

National Aeronautics and
Space Administration

Lewis Research Center
Cleveland, OH 44135-3191